

See discussions, stats, and author profiles for this publication at: <https://www.researchgate.net/publication/359020752>

Prediction of average shape values of quartz particles by vibrating disc and ball milling using dynamic image analysis based on established time-dependent shape models

Article in *Particulate Science And Technology* · March 2022

DOI: 10.1080/02726351.2022.2042879

CITATIONS

2

READS

60

2 authors:



Ugur Ulusoy

Sivas Cumhuriyet University

101 PUBLICATIONS 1,188 CITATIONS

SEE PROFILE



Güler Bayar

Sivas Cumhuriyet University

4 PUBLICATIONS 2 CITATIONS

SEE PROFILE

Some of the authors of this publication are also working on these related projects:



Frontiers' Research Topic [View project](#)



Graduate thesis project [View project](#)



Prediction of average shape values of quartz particles by vibrating disc and ball milling using dynamic image analysis based on established time-dependent shape models

Ugur Ulusoy & Guler Bayar

To cite this article: Ugur Ulusoy & Guler Bayar (2022) Prediction of average shape values of quartz particles by vibrating disc and ball milling using dynamic image analysis based on established time-dependent shape models, *Particulate Science and Technology*, 40:7, 870-886, DOI: [10.1080/02726351.2022.2042879](https://doi.org/10.1080/02726351.2022.2042879)

To link to this article: <https://doi.org/10.1080/02726351.2022.2042879>



Published online: 04 Mar 2022.



Submit your article to this journal [↗](#)



Article views: 240



View related articles [↗](#)



View Crossmark data [↗](#)



Prediction of average shape values of quartz particles by vibrating disc and ball milling using dynamic image analysis based on established time-dependent shape models

Ugur Ulusoy^{a,b}  and Guler Bayar^{a,c} 

^aMining Engineering Department, Sivas Cumhuriyet University, Sivas, Turkey; ^bChemical Engineering Department, Sivas Cumhuriyet University, Sivas, Turkey; ^cNanotechnology Engineering Department, Sivas Cumhuriyet University, Sivas, Turkey

ABSTRACT

Although grinding kinetics has been the subject of many researches, there is no research examining the shape kinetics of particles ground by different mills using dynamic image analysis (DIA) in the literature. In this investigation, how the shapes of quartz particles change over time at two different size fractions in two different mills is modeled using the latest image analysis technique, since particle shape of mineral is important in flotation and hydraulic fracturing processes. Empirical time-dependent shape models based on the correlation between average circularity (C_{av}) and bounding rectangle aspect ratio ($BRAR_{av}$) parameters and grinding time for vibratory disc mill and ball milled particles are established with high R^2 values by different fitting. Furthermore, average shape values of particles ground by the mills depending on grinding time were predicted for two size fractions. It was found that, C_{av} data can be better described by linear fitting equations, on the other hand $BRAR_{av}$ data can be better represented by power fitting equations. Since predicted and measured shape values were found close to each other, this approach provides useful information for estimating the milling time required to produce the particles by milling (with less energy and cost) appropriately for intended use.

KEYWORDS

Quartz; shape; dynamic image analysis; circularity; vibratory disc mill; ball mill

1. Introduction

While silica sand can be generally termed as a natural quartz sand that is 0.074–4.76 mm, products are usually named for their intended use (Ciullo 1996). For instance, frac sand, which consists mostly of quartz particles, is used as a “proppant” in the hydraulic fracturing process to penetrate and provide boreholes through which oil or gas can flow to a well (Mitchell 2015).

Since high-purity quartz is a crucial high-tech raw material widely used in many industries such as microelectronics, integrated circuits, optical fibers, solar cells, electro-magnetic materials, aerospace and military (Tuncuk and Akcil, 2014), quartz ores are generally enriched by flotation as well as magnetic separation and acid-cleaning (Sayilgan and Arol 2004; Sekulic et al. 2004; Wang and Ren 2005; Mowla, Karimi, and Ostadnezhad 2008). It has been reported that, more than 2 billion tons of minerals and fine coals are being treated annually by using flotation technique in worldwide (Nguyen and Schulze 2004). This means huge quantity of fine particles should be created by grinding before flotation. In order to reduce excess energy consumption and global warming, grinding with a suitable mill for sufficient time becomes very important as it accounts for 4% of global energy use.

Dynamic image analysis (DIA), which was used as the most accurate tool for the characterization of differently ground mineral particles in our previously published papers (Ulusoy and Igathinathane 2014; Ulusoy 2018, 2019; Ulusoy and Yekeler 2014) indicates that different grinding cause different shape of particles. So, when quartz material is subjected to milling operation for size reduction prior to beneficiation, the morphological characters of the particles also change depending on grinding time as well as applied forces acting in the mill. It is well known that, particle shape is one of the affecting physical variables of solid on the separation processes like flotation (Trahar and Warren 1976; Wotruba, Hoberg, and Schneider 1991; Hıçyılmaz, Ulusoy, and Yekeler 2004; Rahimi et al. 2012; Verrelli et al. 2014; Wang et al. 2020). Moreover, studies suggesting that the flotation rate and recovery increase with the increase of the elongation ratio have increased considerably recently (Ulusoy, Yekeler, and Hıçyılmaz 2003; Koh et al. 2009; Guven et al. 2016; Ma, Xia, and Xie 2018). On the other hand, frac sand particles must have a good roundness to assure that they flow unhindered into the fractures (Mitchell 2015). Therefore, it is important to use a more suitable grain-shaped mill product for intended use. It has been reported that, product shape of targeted minerals such as quartz, magnetite, South African platinum group and gold can be generated by utilizing

suitable mills (Hiçyılmaz, Ulusoy, and Yekeler 2004; Ofori-Sarpong and Amankwah 2011; Dehghani, Rahimi, and Rezai 2012; Rahimi et al. 2012; Little et al. 2017). So, a better flotation separation performance could be achieved by selecting proper milling system and sufficient grinding time. Thus, the rate of change in shape of particles created by different grinding is a valuable information for predicting the required grinding time, choosing a suitable mill as well as predicting behavior of minerals ground in subsequent process (Choi et al. 2013). Considering energy and cost saving during milling of industrial minerals, this approach can be used to determine the required grinding time for targeted shape of particles using more appropriate mill for intended use.

Although particle size is closely related to shape, most of the previously published research has been focused on changes in particle size, distributions and breakage behaviors as a function of grinding time (Austin and Bagga 1981; Teke et al. 2002), no attempts were done to investigate the rate of change in shape of quartz particles created by different mill types and grinding time especially using *DIA*. If prediction of the shape changes can be made based on a mathematical model and how predicted results approach to the experimental values, this could be useful for obtaining required shape to better flotation according to calculated grinding time. Therefore, the aims of this study are three-fold: (i) to investigate the impact of the mill types and grinding time on the shape distribution (*sd*) of quartz particles ground by vibratory disc mill and ball mill using *DIA*; (ii) to find out the rate of shape changes of differently ground particles by incremental grinding approach at similar size by correlating the average shape values with time; and (iii) to establish empirical time-dependent models between average shape parameters of ground particles and grinding time for the prediction of average shape values from selected mills as well as prediction of grinding time for required particles shape in flotation as well as hydraulic fracturing process.

2. Theoretical background for dynamic image analysis

Image analysis, which is the recent technique for characterization of particle morphology, can be performed as either static or dynamic. Whilst particles are measured in random orientation (3 dimensions) in dynamic method, particles are detected in stable orientation (2 dimensions) in static method. Therefore, *DIA* can give valuable information for comparison of *sd* for differently ground minerals at the same sizes. Working principle of *DIA* is based on recording of particle silhouettes by the camera while particles are moving downwards in a flow cell between light source and camera as illustrated by Figure 1.

Particle shape of ground mineral particles can be best described by Circularity (*C*) and Bounding Rectangle Aspect Ratio (*BRAR*) (Micromeritics 2013) as in the following Equations (1) and (2):

$$C = (4A)/\pi(D_{BC}^2) \quad (1)$$

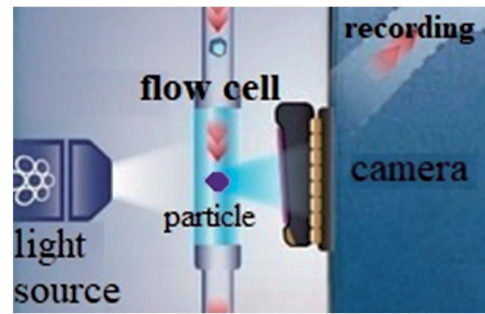


Figure 1. Working principles of *DIA* (modified from Vision Analytical Inc., 2021).

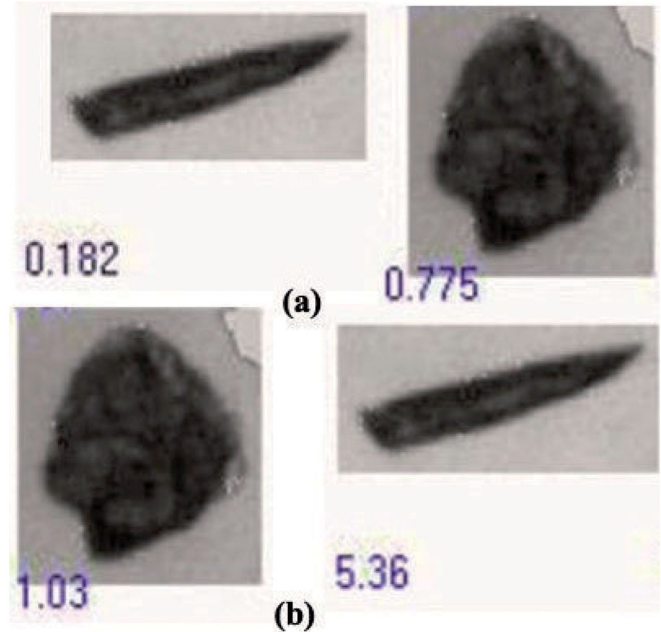


Figure 2. (a) *C* and (b) *BRAR* values measured for the same spherical and elongated ground quartz particles by *DIA* in this study.

$$BRAR = (BRL/BRW) \quad (2)$$

where, *A* is the area of the particle image, D_{BC} is bounding circle diameter, *BRL* is bounding rectangle length, and *BRW* is bounding rectangle width. *C* takes a value between 1 and 0 while *BRAR* takes always greater than 1. It should be noted that, *C* takes a maximum value of 1, but *BRAR* takes a minimum value of 1 for a perfect circle. As the shape of particle deviates from sphere to elongated, the value of *C* is decreasing down to 0, whereas the value of *BRAR* is increasing from 1, as clearly seen from Figure 2.

3. Materials and methods

3.1. Sample preparation and grinding tests

High grade quartz (97% SiO₂) from Turkey was used for this study to quantify shape of particles created by incremental grinding of vibratory disc mill and ball mill. For this aim, the particle size of bulk quartz materials (approximately 10 cm in size) was firstly reduced by jaw crusher. Then, crushed materials were screened at 10 min, which was determined as optimum previously (Ulusoy, Yekeler, and Hicyi



Figure 3. (a) Quartz sample prepared as 0.600–0.850 mm size fraction (b) ball mill (c) vibratory disc mill (d) sieving shaker used for the sample preparation.

Imaz 2003) to prepare 0.600–0.850 mm feed fractions for ring and ball milling (Figure 3(a)).

In order to investigate the effect of mill type, grinding time on the particle's shapes generated by incremental grinding, two different mills having different grinding mechanisms were used in this study, i.e., a ball mill for a tumbling mill and a vibratory disc mill for a non-tumbling mill.

A laboratory vibratory disc mill (Ünal Mühendislik, Turkey), which is a high-speed multi-amplitude vibration machine is generally used for sample preparation before X-ray fluorescence, X-ray diffraction and atomic absorption analysis due to ease of operation and faster grinding. It has a diameter of 18.8 and height of 6 cm. vibratory disc milling (Figure 3(c)) tests were conducted in a 500 mL volume of puck using 7.4, 9.4 and 14 cm diameters of rings with a material charge of 100.0 g of 0.600–0.850 mm size fraction.

On the other hand, dry ball milling tests were carried out in a laboratory ball mill having a 20 cm internal diameter and 5776 cm³ volume (Figure 3(b)) with charge of 5475 g steel ball mixtures (30 and 26 mm in diameter) and 359.5 g material (0.600–0.850 mm), respectively. Although quartz is a well-known brittle material widely used for breakage tests, a loading of 20% of the mill volume filled by the ball bed, fractional powder filling of 0.04 and a fractional interstitial filling of the bed voids by the dry powder of 0.5 at 75% of the critical speed (77 rpm) were used for a normal first-order breakage (Yekeler, Özkan, and Austin 2001).

For incremental grinding approach used in this study, grinding times were set at 10, 20, 30, 40, 50 and 60 sec for vibratory disc milling and 1, 2, 5, 10, 20 and 40 min (or 60,

120, 300, 600, 1200 and 2400 sec) for ball milling. Since vibratory disc mill can produce too small particles in a very short time compared to ball mill (Ulusoy and Igathinathane 2016), very short grinding time intervals were used for vibratory disc milling in order to produce shape variation. Since best size fraction in flotation is 0.053–0.250 mm as well as in the measurement of *DIA*, the particulate materials were dry screened through 250, 150 and 53 μ m sieves after each grinding at specified time. So that two closed sized fractions (0.150–0.250 mm and 0.053–0.150 mm) were prepared for *DIA* (Figure 3(d)) by using Retch laboratory standard sieves using Endecotts sieve shaker (Octagon 200, Endecotts Ltd, UK) at screening conditions of 10 min, 40 amplitude and continuous frequency.

3.2. Dynamic image analysis tests

In order to prepare a few g of representative sample for *DIA*, rotary spinning riffler (Quantachrome[®] Instruments), which is considered as the most reliable sampling technique (Allen 1997) was used (Figure 4). Once representative sample was put in a glass beaker, which is full of 25 ml water, it was hold in the ultrasonic bath at 5 min. Then, a few drops from well dispersed suspension were used for *DIA* (Micromeritics[®] Instrument Corp., Norcross, USA) for particle shape characterization as given in Table 1.

Although dynamic imaging, thanks to superior features of sample recirculation and random orientation, gives shape data in terms of *C* and *BRAR* shape parameters for each sample along with distribution statistics and thumbnail

Experimental scheme for DIA



Rotary spinning riffler

Ultrasonic treatment

DIA

Figure 4. Dynamic image analysis procedure followed for this study.

Table 1. System summary for DIA measurements.

System	Variable	Value
Pump	Speed (% of max)	40
Rinse	Drain pump speed (%)	50
	Fill pump speed (%)	40
	Drain time (sec)	15
	Fill time (sec)	10
	Number of cycles	3
Debubble	Pause time (sec)	0
	Run time (sec)	1
	Number of cycles	0
Dilution	Percent	100
Camera	Gain (as a % of max)	80
	Brightness baseline (as a % of max)	0
Calibration	Micron/pixel ratio	1.300
	Magnification	5.69
	Image size (microns)	1664 × 1248
Instrument hardware	Pump speed %	40
	Camera gain %	80
Concentration	Particles/frame	1.94
	Flow cell depth (mm)	0.50
	Probe volume (mm ³)	1.038
	Part./ml (measured)	1.866E + 03
	Dilution (%)	100
	Part./ml (original)	1.866E + 03
	Dark pixel %	1.35
System indicators	In-focus count	10,002
	Video frames	5161
	Run time (sec)	506
	Focus reject %	0
	Shape reject %	0
	Border reject %	0.8
	Average background intensity	180

images (Vision Analytical Inc 2020), each measurement was conducted as 3 series by counting more than 10,000 particles per each run and the results were reported as the mean values of three such sets.

4. Results and discussion

4.1. Dynamic image analysis tests results

The repeatability test of DIA results for each mill product at each size fraction was performed and given in Figure 5,

indicating that 3 repetitions are consistent each other. It was found that, C increases as grinding time increases (Figure 5(a-d)) whereas, $BRAR$ decreases as grinding time increases (Figure 5(e-h)) for vibratory disc and ball milling.

Since ring mill grinds faster than ball mill, shape changes were compared based on time durations of 10, 20, 30, 40, 50 and 60 sec for vibratory disc milled particles and 60, 120, 300, 600, 1200 and 2400 sec for ball milled particles, respectively, considering fineness of the mill products. For example,

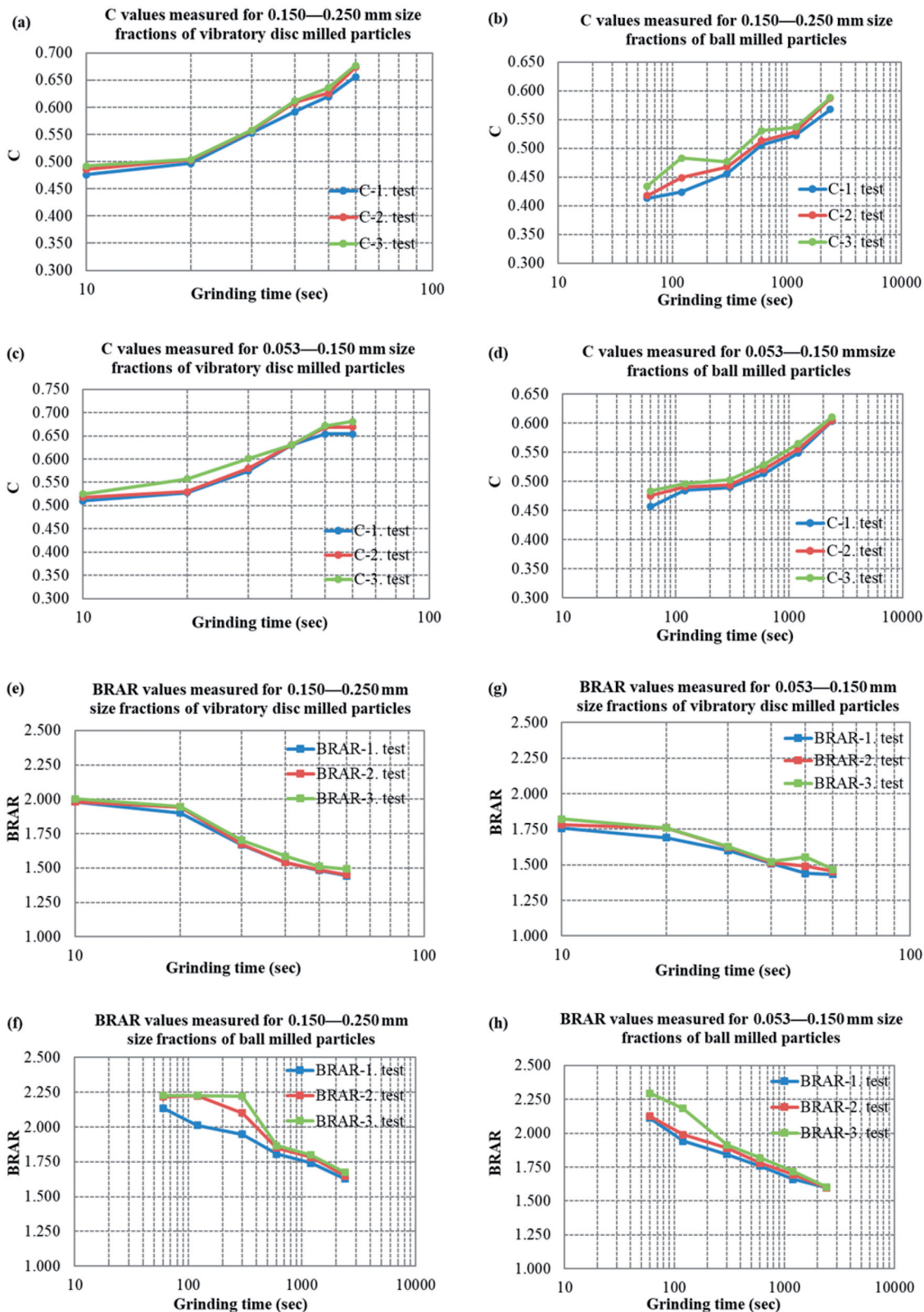


Figure 5. The repeatability test of DIA results for each mill product, (a) C values (0.150–0.250 mm), as a function of vibratory disc milling time (b) C values (0.150–0.250 mm) as a function of ball milling time, (c) C values (0.053–0.150 mm) as a function of vibratory disc milling time, (d) C values (0.053–0.150 mm) as a function of ball milling time, (e) $BRAR$ values (0.150–0.250 mm) as a function of vibratory disc milling time, (f) $BRAR$ values (0.150–0.250 mm) as a function of ball milling time, (g) $BRAR$ values (0.053–0.150 mm) as a function of vibratory disc milling time, (h) $BRAR$ values (0.053–0.150 mm) as a function of ball milling time.

10 sec vibratory disc milled particles was compared 60 sec ball milled particles as the time duration 1. Average values of C ($C_{av.}$) and $BRAR$ ($BRAR_{av.}$) parameters measured by 3 repetition (Figure 5) for vibratory disc and ball milled

particles at two size fractions were compared as given in Figure 6. It is found that $C_{av.}$ values of vibratory disc milled particles for both size fractions are higher than those of ball milled particles whereas, $BRAR_{av.}$ values of ball milled

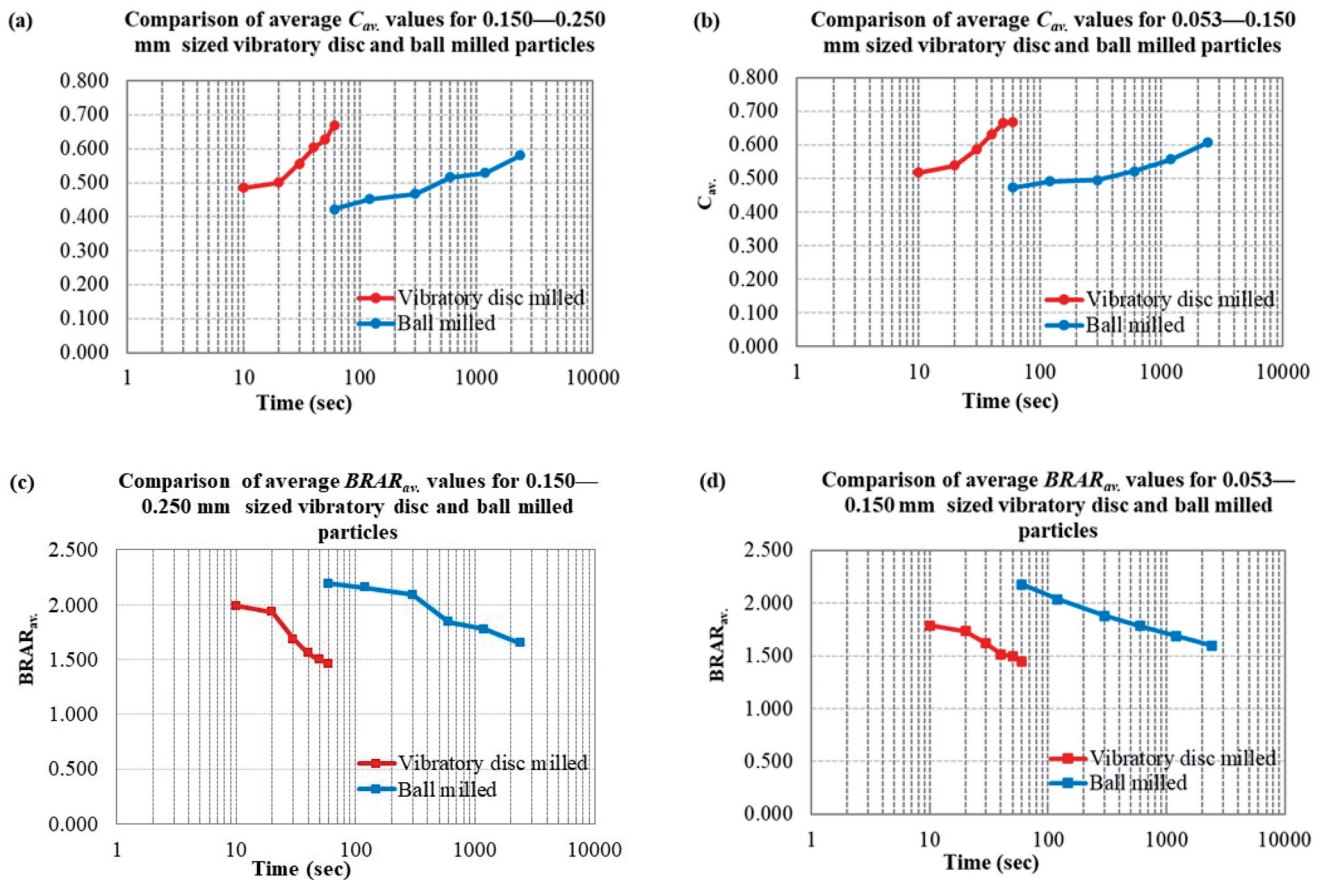


Figure 6. Comparison of average shape values as a function of grinding time periods for vibratory disc and ball milled quartz particles (a) $C_{av.}$ values for 0.150–0.250 mm size fraction, (b) $C_{av.}$ values for 0.053–0.150 mm size fraction, (c) $BRAR_{av.}$ values for 0.150–0.250 mm size fraction, (d) $BRAR_{av.}$ values for 0.053–0.150 mm size fraction.

particles for both size fractions are higher than those of vibratory disc milled particles since dominant forces acted in vibratory disc and ball milling are attrition and impact, respectively. It can be clearly seen from the Figure 6 that, particle shape of both mill products as a function of grinding time are obviously different for both size fractions. It is found that $C_{av.}$ increasing with time and $BRAR_{av.}$ decreasing with time. This indicates that particle shape of both mill products is getting rounder and rounder. In addition, vibratory disc milled particles (due to attrition) had more rounded particles than ball milled particles for each size fraction. This was supported by Figure 7, which illustrates thumbnail images of vibratory disc and ball milled particles at the lowest and the highest grinding time for both size fractions. As clearly seen from Figure 7(a–d), vibratory disc and ball milled particles at the lowest time (10 sec for vibratory disc milling and 60 sec ball milling) for both size fractions are highly elongated and sharp edged, since mill feed materials were prepared by jaw crusher. Because jaw crusher has compression loading mechanism (Unland 2007), which affect the particle surface and creates new corners. Although thumbnail images of 0.053–0.150 mm size fractions (Figure 7(e–h)) have the smallest particles than those of 0.053–0.150 mm size fractions (Figure 7(a–d)), vibratory disc milled particles at both size fractions are more rounded

than ball milled particles due to the attrition. This is in good agreement with previous reported study (Kaya, Hogg, and Kumar 2002; Ulusoy and Igathinathane 2014; Petrakis et al. 2019) indicating that continued exposure to the grinding environment leads to rounding of the particles. Figure 8 indicates that particles are well dispersed for the measurement by DIA, and also supports the results given in Figure 7. It can be clearly seen from Figure 8 that the shape of particles getting rounder and rounder. This was attributed to the more attrition forces acting in vibratory disc mill compared to ball mill, which has impact force as dominant.

Changes in particle shape of ring and ball milled quartz particles as a function of grinding time was given in Figure 9. While $C_{av.}$ values of both size fractions gradually increased with grinding time for vibratory disc and ball mill, $BRAR_{av.}$ values of both size fractions decreased with grinding time. Since $C_{av.}$ values of vibratory disc milled particles are higher than those of ball milled particles, vibratory disc milled particles are much more rounded than ball milled particle for both size fractions, namely 0.150–0.250 mm and 0.053–0.150 mm. Conversely, ball milled particles have higher $BRAR_{av.}$ values than vibratory disc milled particles indicating that ball milled particles are more elongated than vibratory disc milled particles due to impact forces played role on ball milling.

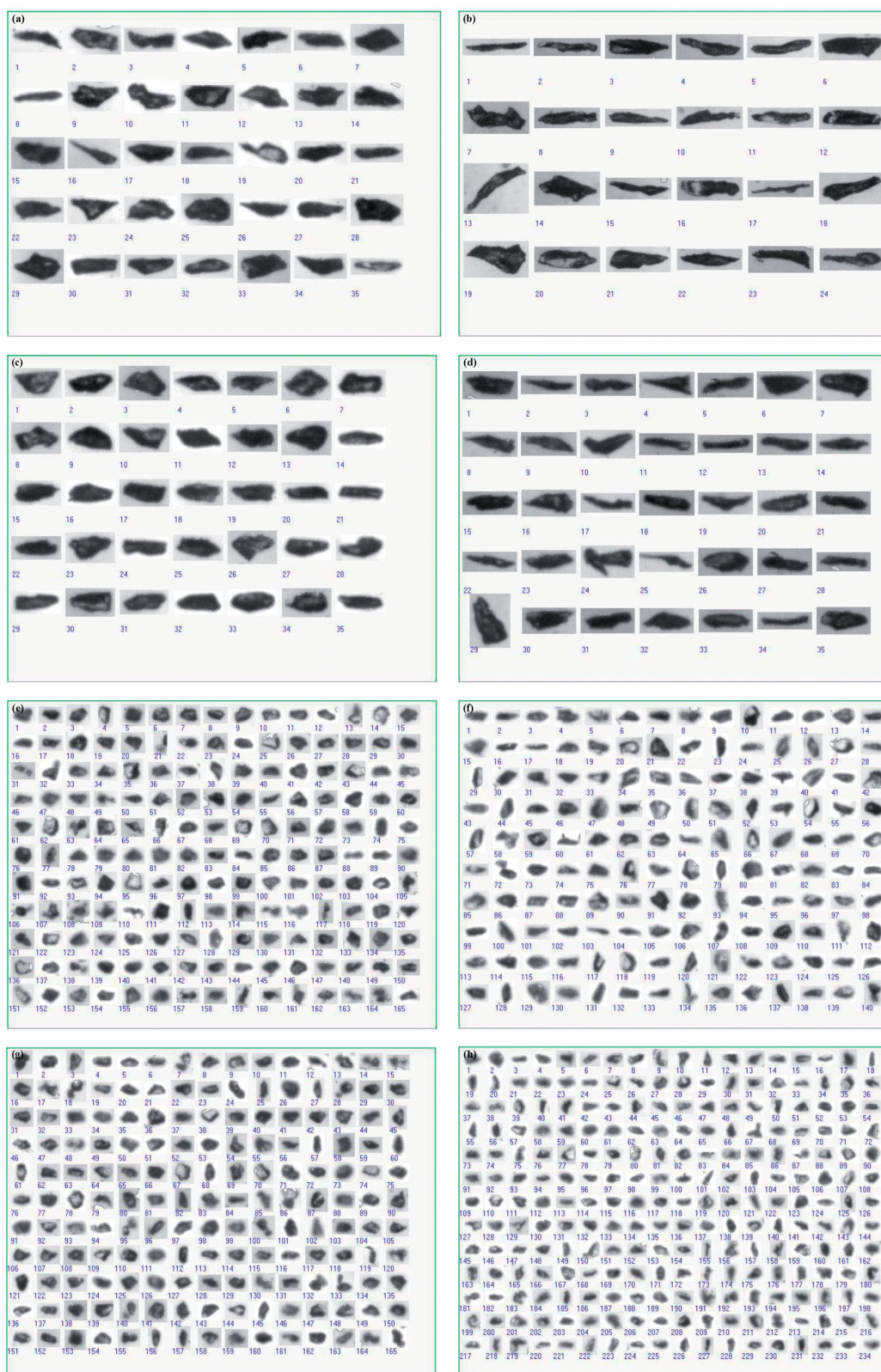


Figure 7. Thumbnail images of vibratory disc milled (10 and 60 sec) and ball milled (60 and 2400 sec) particles at 0.150–0.250 mm and 0.053–0.150 mm size fractions, (a) *sd* of vibratory disc milled (10 sec) particles at 0.150–0.250 mm size fraction (b) *sd* of ball milled (60 sec) particles at 0.150–0.250 mm size fraction, (c) *sd* of vibratory disc milled (10 sec) particles at 0.053–0.150 mm size fraction (d) *sd* of ball milled (60 sec) particles at 0.053–0.150 mm size fraction, (e) *sd* of vibratory disc milled (60 sec) particles at 0.150–0.250 mm size fraction, (f) *sd* of ball milled (2400 sec) particles at 0.150–0.250 mm size fraction, (g) *sd* of vibratory disc milled (60 sec) particles at 0.053–0.150 mm size fraction, (h) *sd* of ball milled (2400 sec) particles at 0.053–0.150 mm size fraction.

Up to now DIA, which was found as the most accurate tool for the characterization of differently ground mineral particles in our previously published papers (Ulusoy and

Igathinathane 2014; Ulusoy and Yekeler 2014; Ulusoy 2018; 2019) indicates that shape of particles obtained by different grinding system is not the same due to different breakage

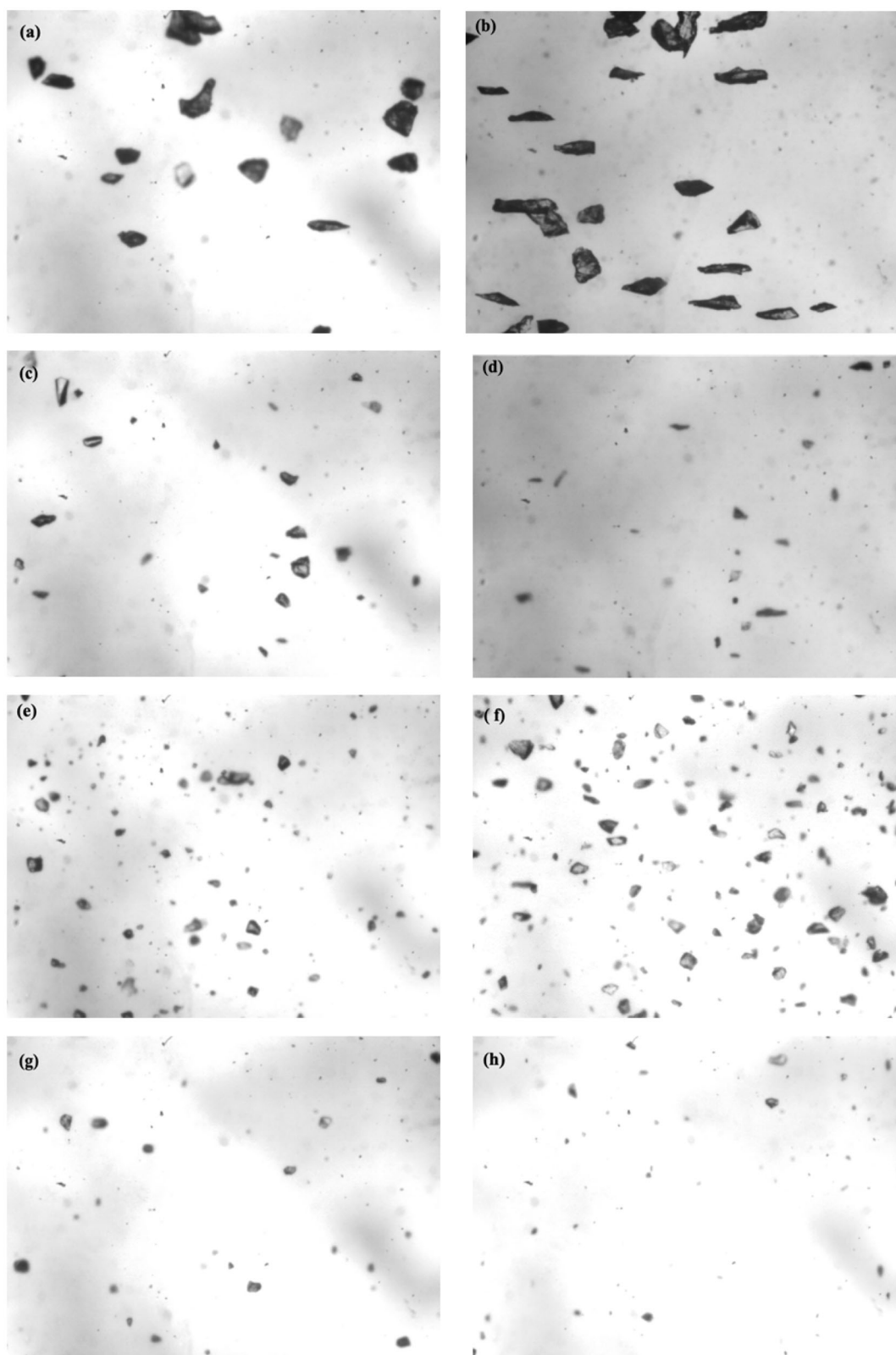


Figure 8. DIA images recorded for at the lowest and the highest grinding time for both size fractions a) images of vibratory disc milled (10 sec) particles at 0.150–0.250 mm size fraction, (b) images of ball milled (60 sec) particles at 0.150–0.250 mm size fraction, (c) images of vibratory disc milled (10 sec) particles at 0.053–0.150 mm size fraction, (d) images of ball milled (60 sec) particles at 0.053–0.150 mm size fraction, (e) images of vibratory disc milled (60 sec) particles at 0.150–0.250 mm size fraction, (f) images of ball milled (2400 sec) particles at 0.150–0.250 mm size fraction, (g) images of vibratory disc milled (60 sec) particles at 0.053–0.150 mm size fraction, (h) images of ball milled (2400 sec) particles at 0.053–0.150 mm size fraction.

forces acted in the mills. As clearly seen from [Figure 9](#), particle shape changes gradually from elongated to rounded with grinding time. This could be useful for

obtaining required shape for intended use, when the required grinding time is predicted from time-dependent shape models.

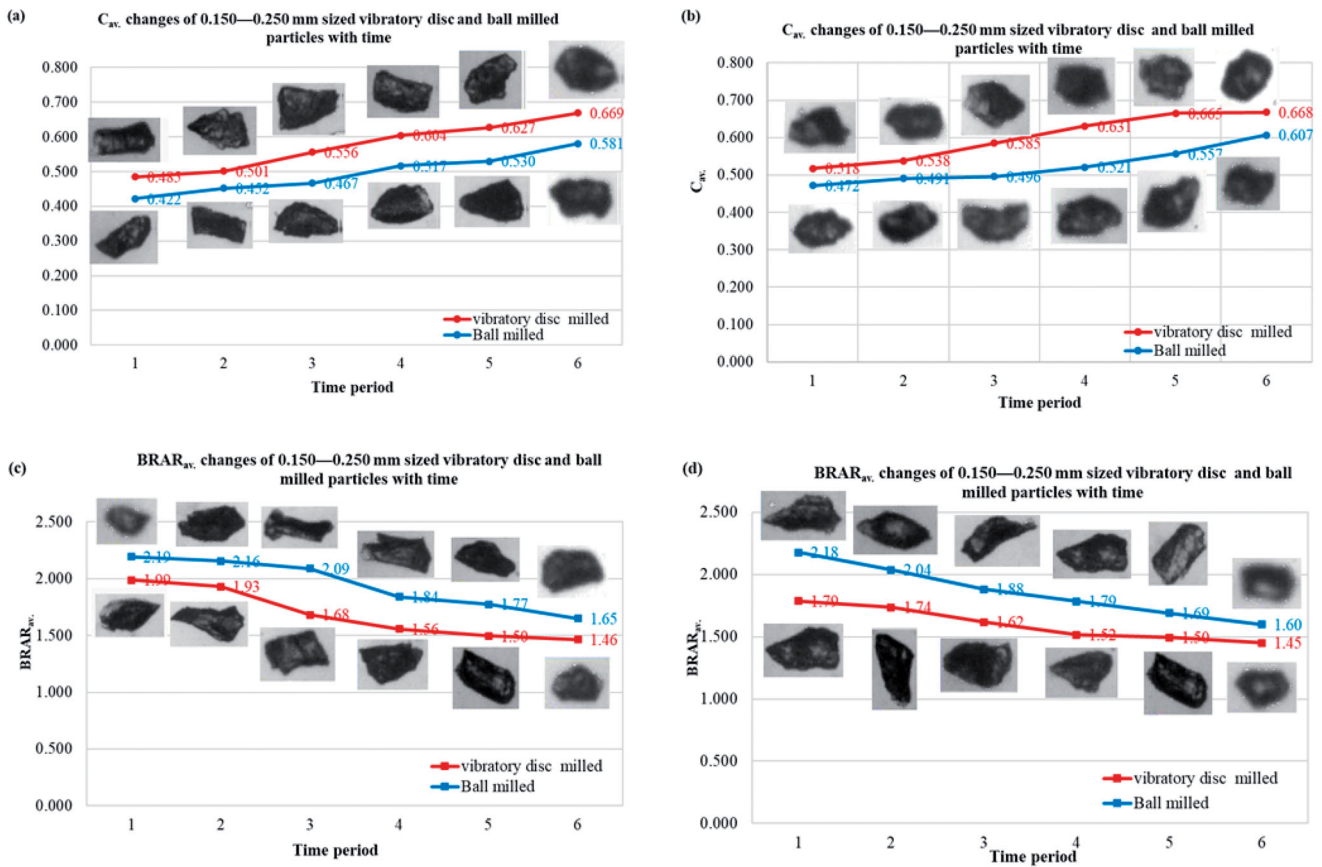


Figure 9. Overall change in particle shape of vibratory disc and ball milled quartz with incremental grinding time periods, (a) C_{av} changes of vibratory disc and ball milled particles for 0.150–0.250 mm size fractions, (b) C_{av} changes of vibratory disc and ball milled particles for 0.053–0.150 mm size fractions, (c) $BRAR_{av}$ changes of vibratory disc and ball milled particles for 0.150–0.250 mm size fractions, (d) $BRAR_{av}$ changes of vibratory disc and ball milled particles for 0.053–0.150 mm size fractions. Note: Time period 1 refers to 10 and 60 sec for vibratory disc and ball milling, respectively. Time period 2 refers to 20 and 120 sec for vibratory disc and ball milling, respectively. Time period 3 refers to 30 and 300 sec for vibratory disc and ball milling, respectively. Time period 4 refers to 40 and 600 sec for vibratory disc and ball milling, respectively. Time period 5 refers to 50 and 1200 sec for vibratory disc and ball milling, respectively. Time period 6 refers to 60 and 2400 sec for vibratory disc and ball milling, respectively.

4.2. Predicted versus experimental shape values

In this section, correlations of average shape values of vibratory disc and ball milled quartz particles with grinding time by linear fitting (C_{av} and $BRAR_{av}$) and an alternative fitting model (exponential for C_{av} and power functions for $1/BRAR_{av}$) were compared based on the highest R^2 value of all the alternative fitting models tested. The established equations along with R^2 values were given in Table 2. The experimental and predicted values of C_{av} and $BRAR_{av}$ depending on various grinding time for both size fractions with the absolute % and relative % errors were summarized in Tables 3 and 4.

In linear fitted model, the established empirical time-dependent shape models for the correlations between C_{av} and grinding time for vibratory disc and ball milled particles are in the form of “ $C_{av} = a.t + b$ ” while the correlations between $BRAR_{av}$ and grinding time for vibratory disc and ball milled particles are in the form of “ $BRAR_{av} = -a.t + b$ ” type equations (where a and b are constants) as shown in Figure 10). The minimum R^2 value was obtained as 0.739 for ball milling at finer size fraction, on the other hand the maximum value was predicted as 0.984 for vibratory disc milling at coarser size fraction. It was found that R^2 values

of established empirical models for vibratory disc milled particles are higher than those of ball milled particles. As clearly seen from Figure 11, predicted and measured C_{av} values were found close to each other with more than 0.92 R^2 values. Besides, C_{av} of 30 sec of vibratory disc milling for both size fractions, 300 sec of ball milling for coarser size fraction and 120 sec of ball milling for finer size fraction were successfully predicted with zero absolute % errors as seen from Table 3. It was also found that relative error values greater than 5% were obtained at ball milling data especially at the longest grinding times. But, $BRAR_{av}$ prediction for ball milled particles at two size fraction is not so strong (Figure 11(f,h)). As can be seen clearly from Table 4, $BRAR_{av}$ of only 2400 sec of ball milling for coarser size fraction was successfully predicted. Relative error values greater than 5% were obtained by 600 and 1200 sec of ball milling.

By exponential fitting for C_{av} and power fitting for $1/BRAR_{av}$, the established empirical time-dependent shape models for the correlations between C_{av} and log time for vibratory disc and ball milled particles are in the form of “ $C_{av} = a.e^{(b.t)}$ ” while the correlations between $1/BRAR_{av}$ and log time for vibratory disc and ball milled particles are in the form of “ $1/BRAR_{av} = a.t^b$ ” type equations (where a and b are constants) as shown in Figure 12. While the

Table 2. Summary of the empirical models established along with their R^2 values.

Fitting type	Size fractions (mm)	Mill product	Equations	R^2
$C_{av.}$ - log(time) exponential fitted and $1/BRAR_{av.}$ - log(time) power fitted	0.150–0.250	Vibratory disc	$C_{av.} = 0.0039 t + 0.439$	0.984
		Ball	$C_{av.} = 0.0001 t + 0.4371$	0.959
	0.053–0.150	Vibratory disc	$C_{av.} = 0.0034 t + 0.4830$	0.962
		Ball	$C_{av.} = 0.0001 t + 0.4809$	0.973
	0.150–0.250	Vibratory disc	$BRAR_{av.} = -0.0116 t + 2.0924$	0.926
		Ball	$BRAR_{av.} = -0.0002 t + 2.1290$	0.827
	0.053–0.150	Vibratory disc	$BRAR_{av.} = -0.0072 t + 1.8514$	0.952
		Ball	$BRAR_{av.} = -0.0002 t + 2.0249$	0.739
	0.150–0.250	Vibratory disc	$C_{av.} = 0.4498e^{0.0068t}$	0.982
		Ball	$C_{av.} = 0.4405e^{0.0002t}$	0.952
	0.053–0.150	Vibratory disc	$C_{av.} = 0.4903e^{0.0057t}$	0.951
		Ball	$C_{av.} = 0.4821e^{0.0001t}$	0.963
	0.150–0.250	Vibratory disc	$1/BRAR_{av.} = 0.312t^{0.191}$	0.940
		Ball	$1/BRAR_{av.} = 0.317t^{0.082}$	0.945
	0.053–0.150	Vibratorydiscmill	$1/BRAR_{av.} = 0.4108t^{0.1242}$	0.944
		Ball	$1/BRAR_{av.} = 0.329t^{0.083}$	0.999

Table 3. Practical application of the $C_{av.}$ prediction model.

Fitting	Size (mm)	Grinding time	Experimental	Predicted	Absol. error*	Rel. error (%)**
Linear	0.150 – 0.250	10 sec Vibratory disc milling	0.485	0.478	0.007	1.376
		20 sec Vibratory disc milling	0.501	0.517	-0.016	-3.125
		30 sec Vibratory disc milling	0.556	0.556	0.000	0.000
		40 sec Vibratory disc milling	0.604	0.595	0.009	1.544
		50 sec Vibratory disc milling	0.627	0.634	-0.007	-1.063
		60 sec Vibratory disc milling	0.669	0.673	-0.004	-0.598
	0.053–0.150	10 sec Vibratory disc milling	0.518	0.517	0.001	0.129
		20 sec Vibratory disc milling	0.538	0.551	-0.013	-2.353
		30 sec Vibratory disc milling	0.585	0.585	0.000	0.000
		40 sec Vibratory disc milling	0.631	0.619	0.012	1.850
		50 sec Vibratory disc milling	0.665	0.653	0.012	1.805
		60 sec Vibratory disc milling	0.668	0.687	-0.019	-2.844
	0.150–0.250	60 sec Ball milling	0.422	0.443	-0.021	-5.083
		120 sec Ball milling	0.452	0.449	0.003	0.642
		300 sec Ball milling	0.467	0.467	0.000	-0.021
		600 sec Ball milling	0.517	0.497	0.020	3.787
		1200 Ball milling	0.530	0.557	-0.027	-5.179
		2400 sec Ball milling	0.649	0.677	-0.028	-4.330
	0.053–0.150	60 sec Ball milling	0.472	0.487	-0.015	-3.084
		120 sec Ball milling	0.491	0.493	-0.002	-0.455
		300 sec Ball milling	0.496	0.511	-0.015	-3.073
		600 sec Ball milling	0.521	0.514	-0.020	-3.753
		1200 sec Ball milling	0.557	0.601	-0.044	-7.946
		2400 sec Ball milling	0.607	0.721	-0.114	-18.764
$C_{av.}$ - log(time) exponential and $1/BRAR_{av.}$ - log(time) power	0.150–0.250	10 sec Vibratory disc milling	0.485	0.481	0.003	0.664
		20 sec Vibratory disc milling	0.501	0.515	-0.014	-2.791
		30 sec Vibratory disc milling	0.556	0.552	0.004	0.793
		40 sec Vibratory disc milling	0.604	0.590	0.014	2.305
		50 sec Vibratory disc milling	0.627	0.632	-0.005	-0.735
		60 sec Vibratory disc milling	0.669	0.676	-0.007	-1.108
	0.053–0.150	10 sec Vibratory disc milling	0.518	0.519	-0.001	-0.269
		20 sec Vibratory disc milling	0.538	0.550	-0.011	-2.075
		30 sec Vibratory disc milling	0.585	0.582	0.003	0.558
		40 sec Vibratory disc milling	0.631	0.616	0.015	2.348
		50 sec Vibratory disc milling	0.665	0.652	0.013	1.958
		60 sec Vibratory disc milling	0.668	0.690	-0.022	-3.327
	0.150–0.250	60 sec Ball milling	0.422	0.446	-0.024	-5.728
		120 sec Ball milling	0.452	0.451	0.001	0.177
		300 sec Ball milling	0.467	0.468	-0.001	-0.158
		600 sec Ball milling	0.517	0.497	0.020	3.872
		1200 Ball milling	0.530	0.560	-0.030	-5.724
		2400 sec Ball milling	0.649	0.712	-0.063	-9.689
	0.053–0.150	60 sec Ball milling	0.472	0.485	-0.013	-2.682
		120 sec Ball milling	0.491	0.488	0.003	0.560
		300 sec Ball milling	0.496	0.497	-0.001	-0.225
		600 sec Ball milling	0.521	0.512	0.009	1.807
		1200 sec Ball milling	0.557	0.544	0.013	2.353
		2400 sec Ball milling	0.607	0.613	-0.006	-0.967

*Absolute error = (experimental-predicted).

**Relative error = [(experimental-predicted)/experimental]*100.

Table 4. Practical application of the $BRAR_{av}$ prediction model.

Fitting	Size (mm)	Grinding time	Experimental	Predicted	Absol. error*	Rel. error (%)**
Linear	0.150–0.250	10 sec Vibratory disc milling	1.989	1.976	0.013	0.650
		20 sec Vibratory disc milling	1.931	1.860	0.070	3.640
		30 sec Vibratory disc milling	1.682	1.744	-0.063	-3.730
		40 sec Vibratory disc milling	1.557	1.628	-0.072	-4.608
		50 sec Vibratory disc milling	1.495	1.512	-0.017	-1.164
		60 sec Vibratory disc milling	1.463	1.396	0.067	4.552
	0.053–0.150	10 sec Vibratory disc milling	1.787	1.779	0.008	0.444
		20 sec Vibratory disc milling	1.737	1.707	0.029	1.685
		30 sec Vibratory disc milling	1.618	1.635	-0.017	-1.075
		40 sec Vibratory disc milling	1.516	1.563	-0.048	-3.149
		50 sec Vibratory disc milling	1.495	1.491	0.004	0.241
		60 sec Vibratory disc milling	1.451	1.419	0.032	2.200
	0.150–0.250	60 sec Ball milling	2.193	2.117	0.076	3.480
		120 sec Ball milling	2.155	2.102	0.050	2.320
		300 sec Ball milling	2.091	2.069	0.022	1.036
		600 sec Ball milling	1.840	2.009	-0.169	-9.165
		1200 sec Ball milling	1.774	1.889	-0.115	-6.463
		2400 sec Ball milling	1.649	1.649	0.000	0.000
	0.053–0.150	60 sec Ball milling	2.179	2.013	0.166	7.609
		120 sec Ball milling	2.038	2.001	0.037	1.836
		300 sec Ball milling	1.882	1.965	-0.083	-4.405
		600 sec Ball milling	1.785	1.905	-0.120	-6.697
		1200 sec Ball milling	1.691	1.785	-0.094	-5.574
		2400 sec Ball milling	1.600	1.545	0.055	3.444
C_{av} - log(time) exponential and $1/BRAR_{av}$ - log(time) power	0.150–0.250	10 sec Vibratory disc milling	0.503	0.484	0.018	3.648
		20 sec Vibratory disc milling	0.518	0.553	-0.035	-6.748
		30 sec Vibratory disc milling	0.595	0.597	-0.003	-0.467
		40 sec Vibratory disc milling	0.642	0.631	0.011	1.747
		50 sec Vibratory disc milling	0.669	0.659	0.010	1.531
		60 sec Vibratory disc milling	0.684	0.682	0.002	0.224
	0.053–0.150	10 sec Vibratory disc milling	0.559	0.547	0.013	2.268
		20 sec Vibratory disc milling	0.576	0.596	-0.020	-3.499
		30 sec Vibratory disc milling	0.618	0.627	-0.009	-1.407
		40 sec Vibratory disc milling	0.660	0.650	0.010	1.551
		50 sec Vibratory disc milling	0.669	0.668	0.001	0.165
		60 sec Vibratory disc milling	0.689	0.683	0.006	0.861
	0.150–0.250	60 sec Ball milling	0.456	0.443	0.012	2.731
		120 sec Ball milling	0.464	0.469	-0.005	-1.158
		300 sec Ball milling	0.478	0.506	-0.028	-5.796
		600 sec Ball milling	0.543	0.536	0.008	1.426
		1200 sec Ball milling	0.564	0.567	-0.003	-0.598
		2400 sec Ball milling	0.606	0.600	0.006	1.041
	0.053–0.150	60 sec Ball milling	0.459	0.462	-0.003	-0.687
		120 sec Ball milling	0.491	0.490	0.001	0.220
		300 sec Ball milling	0.531	0.528	0.003	0.593
		600 sec Ball milling	0.560	0.559	0.001	0.115
		1200 sec Ball milling	0.591	0.593	-0.001	-0.190
		2400 sec Ball milling	0.625	0.628	-0.003	-0.432

*Absolute error = (experimental-predicted).

**Relative error = [(experimental-predicted)/experimental]*100.

minimum R^2 value was obtained as 0.940 for vibratory disc milling at coarser size fraction, the maximum R^2 value was predicted as 0.999 for ball milling at finer size fraction. As seen from the Figure 12(f,h), power fitting described $1/BRAR_{av}$ data very well. Figure 13 shows that the experimental and predicted values are very close to each other. As can be seen from Table 3, C_{av} of 10 sec of vibratory disc milling for coarser size fraction, 10 and 30 sec of vibratory disc milling for finer size fraction, 120 and 300 sec of ball milling for coarser size fraction, 120 and 300 sec of ball milling for coarser size fraction and 300 sec of ball milling for finer size fraction were very closely predicted. Relative error values greater than 5% were obtained by 60, 1200 and 2400 sec of ball milling data for coarser size fractions. On the other hand, $1/BRAR_{av}$ of 60 sec of vibratory disc milling for coarser size fraction, 50 sec of vibratory disc milling for finer size fraction, 10 sec vibratory disc milling for finer size

fraction, 1200 sec of ball milling for both size fractions, 120 and 600 sec of ball milling for finer size fraction were closely predicted (Table 4). Relative error values greater than 5% were obtained only by 300 sec of ball milling for coarser size fraction.

4.3. Testing the models for required grinding times for spherical particles

In order to verify the established empirical models, average shape (C_{av} and $BRAR_{av}$) values were predicted based on the longest experimental grinding time using data for vibratory disc milling at 10, 20, 30, 40, 50 sec and using data for ball milling at 60, 120, 300, 600, 1200, 2400 sec, respectively.

The required times of vibratory disc milling to obtain hypothetically spherical particles ($C_{av} = 1$) using linear

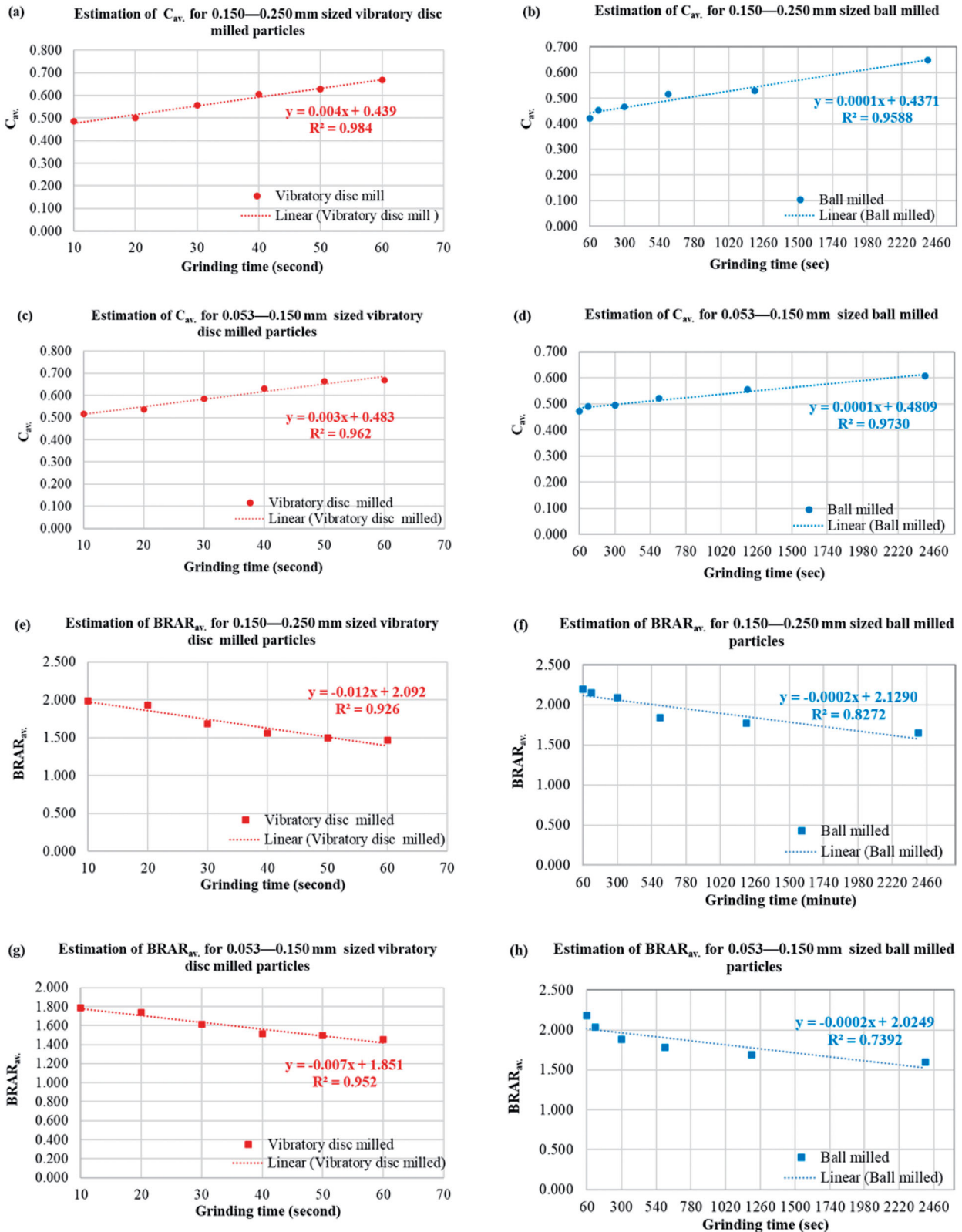


Figure 10. Correlation of average shape values of vibratory disc and ball milled quartz particles with grinding time based on linear fitting (a) C_{av} for vibratory disc milled particles (0.150–0.250 mm), (b) C_{av} for ball milled particles (0.150–0.250 mm), (c) C_{av} for 0.053–0.150 mm sized vibratory disc milled particles, (d) C_{av} for ball milled particles (0.053–0.150 mm), (e) $BRAR_{av}$ for vibratory disc milled particles (0.150–0.250 mm), (f) $BRAR_{av}$ for ball milled particles (0.150–0.250 mm), (g) $BRAR_{av}$ for vibratory disc milled particles (0.053–0.150 mm), (h) $BRAR_{av}$ for ball milled particles (0.053–0.150 mm).

fitted equations ($C_{av} = 0.0039 t + 0.439$ and $C_{av} = 0.0034 t + 0.483$) for 0.150–0.250 mm and 0.053–0.150 mm size fractions were calculated as 144 and 152 sec, respectively. On the other hand, the required times of vibratory disc milling

to obtain hypothetically spherical particles ($BRAR_{av}=1$) using linear fitted equations “ $BRAR_{av} = -0.0116t + 2.0924$ and $BRAR_{av} = -0.0072.t + 1.8514$ ” for 0.150–0.250 mm and 0.053–0.150 mm size fractions were computed as 94 and

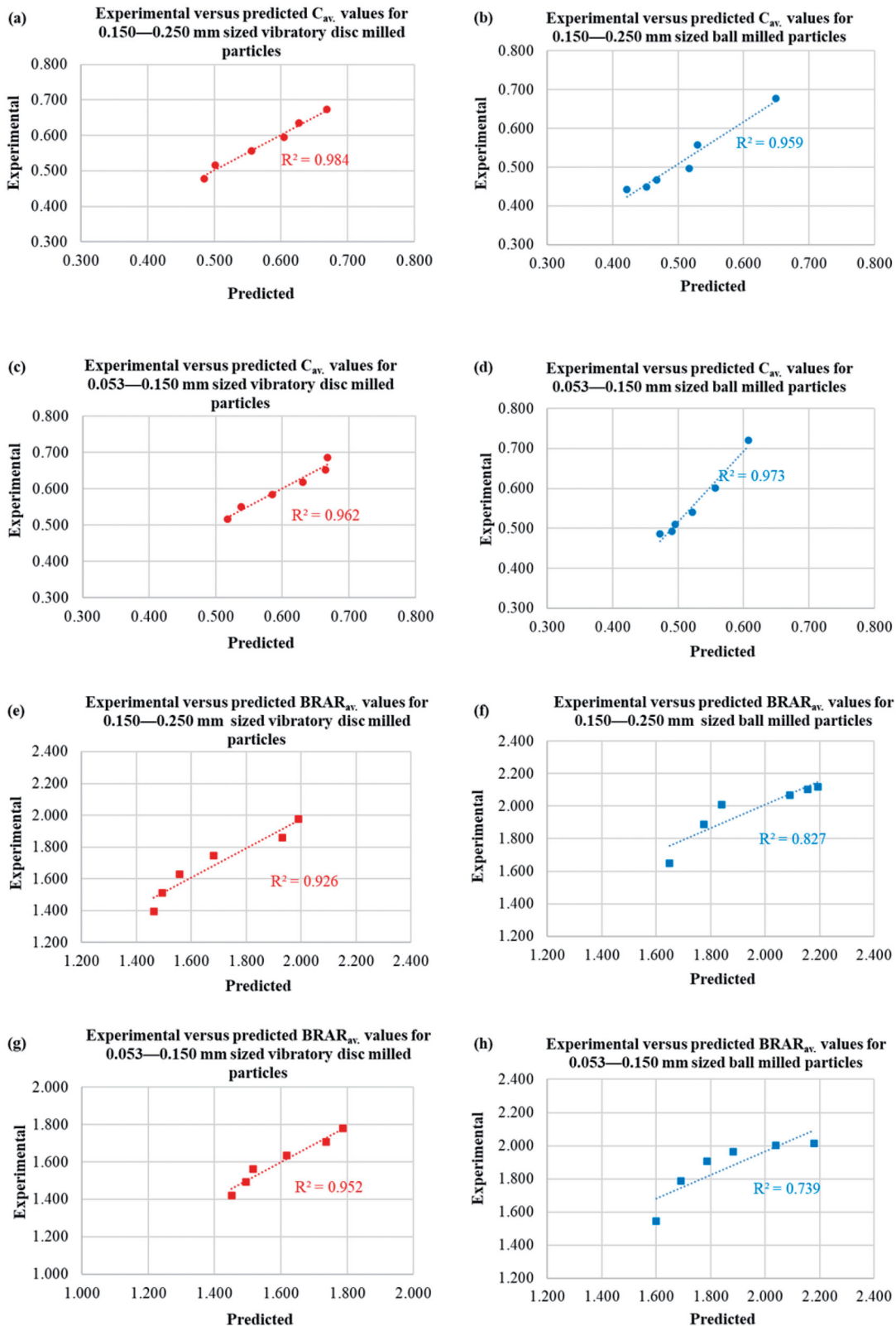


Figure 11. Relationship between predicted and experimental shape values of vibratory disc and ball milled quartz particles for 0.150–0.250 mm and 0.053–0.150 mm size fractions based on linear fitting, (a) C_{av} for vibratory disc milled particles (0.150–0.250 mm), (b) C_{av} for ball milled particles (0.150–0.250 mm), (c) C_{av} for 0.053–0.150 mm sized vibratory disc milled particles, (d) C_{av} for ball milled particles (0.053–0.150 mm), (e) $BRAR_{av}$ for vibratory disc milled particles (0.150–0.250 mm), (f) $BRAR_{av}$ for ball milled particles (0.150–0.250 mm), (g) $BRAR_{av}$ for vibratory disc milled particles (0.053–0.150 mm), (h) $BRAR_{av}$ for ball milled particles (0.053–0.150 mm).

118 sec, respectively. Since very long grinding time of vibratory disc milling would produce too fine particles, which causes agglomeration and sieving problem. In addition, there

will be no sufficient quantity of particles at 0.053–0.150 mm size fraction for sample preparation by screening in order to analyze them by *DIA*. Similarly, the required times of ball



Figure 12. Correlation of C_{av} and $1/BRAR_{av}$ values of vibratory disc and ball milled quartz particles with grinding (log) time based on exponential and power fitting, respectively), (a) C_{av} for vibratory disc milled particles (0.150–0.250 mm), (b) C_{av} for ball milled particles (0.150–0.250 mm), (c) C_{av} for 0.053–0.150 mm sized vibratory disc milled particles, (d) C_{av} for ball milled particles (0.053–0.150 mm), (e) $BRAR_{av}$ for vibratory disc milled particles (0.150–0.250 mm), (f) $BRAR_{av}$ for ball milled particles (0.150–0.250 mm), (g) $BRAR_{av}$ for vibratory disc milled particles (0.053–0.150 mm), (h) $BRAR_{av}$ for ball milled particles (0.053–0.150 mm).

milling to obtain hypothetically spherical particles ($C_{av} = 1$) using linear fitted equations ($C_{av} = 0.0001t + 0.4371$ and $C_{av} = 0.0001t + 0.4809$) for 0.150–0.250 mm and 0.053–0.150 mm size fractions were estimated as 5629 and

5186 sec, respectively. Moreover, the required times of ball milling to obtain hypothetically spherical particles ($BRAR_{av} = 1$) using linear fitted equations ($BRAR_{av} = -0.0002t + 2.129$ and $BRAR_{av} = -0.0002t + 2.0249$) for

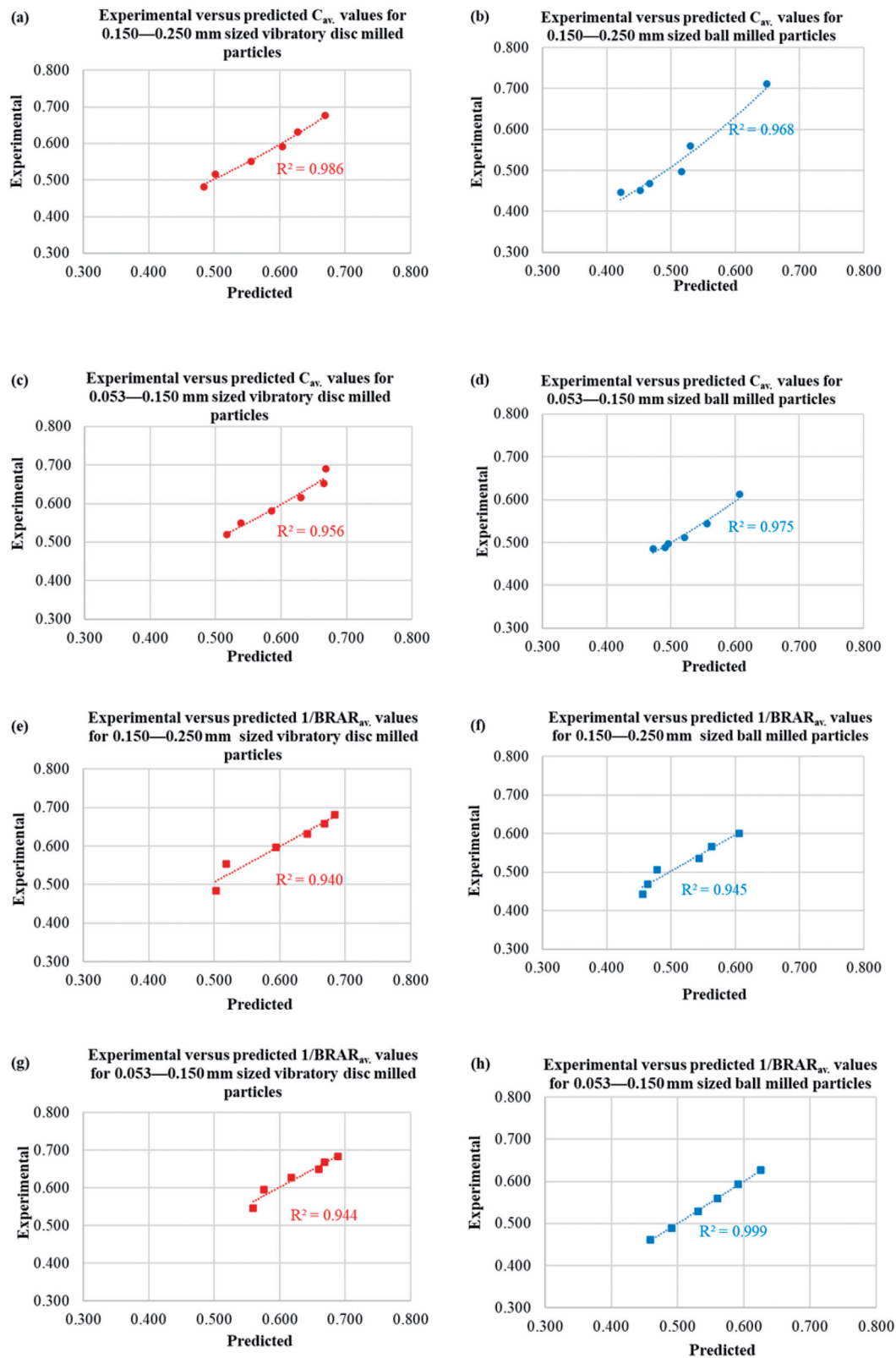


Figure 13. Relationship between predicted and experimental shape values of vibratory disc and ball milled quartz particles for 0.150–0.250 mm and 0.053–0.150 mm size fractions (based on C_{av} – log(time) exponential fitting and $1/BRAR_{av}$ – log(time) power fitting), (a) C_{av} for vibratory disc milled particles (0.150–0.250 mm), (b) C_{av} for ball milled particles (0.150–0.250 mm), (c) C_{av} for 0.053–0.150 mm sized vibratory disc milled particles, (d) C_{av} for ball milled particles (0.053–0.150 mm), (e) $BRAR_{av}$ for vibratory disc milled particles (0.150–0.250 mm), (f) $BRAR_{av}$ for ball milled particles (0.150–0.250 mm), (g) $BRAR_{av}$ for vibratory disc milled particles (0.053–0.150 mm), (h) $BRAR_{av}$ for ball milled particles (0.053–0.150 mm).

0.150–0.250 mm and 0.053–0.150 mm size fractions were predicted as 5643 and 5123 sec, respectively. These predicted values correspond to more than 85 minute of ball milling,

which causes agglomeration, and problems in the processes of sieving and grinding. Besides, there will be no sufficient quantity of particles at 0.053–0.150 mm size fraction for

sample preparation by screening in order to analyze them by *DIA*.

The required grinding times of vibratory disc milling to obtain hypothetically spherical particles ($C_{av.} = 1$) using exponential fitting for $1/BRAR_{av.}$ equations ($C_{av.} = 0.4498e^{0.0068t}$ and $C_{av.} = 0.4903e^{0.0057t}$) for 0.150–0.250 mm and 0.053–0.150 mm size fractions were calculated as 118 and 126 sec, respectively. But, the required times of vibratory disc milling to obtain hypothetically spherical particles ($BRAR_{av.}=1$) using linear fitted equations ($1/BRAR_{av.} = 0.312t^{0.191}$ and $1/BRAR_{av.} = 0.4108t^{0.1242}$) for 0.150–0.250 mm and 0.053–0.150 mm size fractions were computed as 444 and 1290 sec, respectively. This means very long grinding time of vibratory disc milling, which would produce too fine particles. Therefore, it will cause agglomeration and sieving problem. In addition, there will be no sufficient quantity of particles at 0.053–0.150 mm size fraction for sample preparation by screening in order to analyze them by *DIA*.

With the same approach, the required times of ball milling to obtain hypothetically spherical particles ($C_{av.} = 1$) using linear fitted equations ($C_{av.} = 0.4405e^{0.0002t}$ and $C_{av.} = 0.4821e^{0.0001t}$) for 0.150–0.250 mm and 0.053–0.150 mm size fractions were forecasted as 4100 and 7300 sec, respectively. These results, which correspond to 68 minute and 121 minute of ball milling are reasonable prediction to attain. On the other hand, the required times of ball milling to obtain hypothetically spherical particles ($BRAR_{av.}=1$) using linear fitted equations ($1/BRAR_{av.} = 0.317t^{0.082}$ and $1/BRAR_{av.} = 0.329t^{0.083}$) for 0.150–0.250 mm and 0.053–0.150 mm size fractions are not reasonable (120990 and 659000 sec, respectively).

5. Conclusion

Determination of shape kinetics of quartz particles ground by vibratory disc and ball milling at two size fractions by incremental grinding approach was successfully performed by utilizing the latest imaging technique called *DIA*. It was concluded that, the average shape of particles for both mill products changed widely from elongated to round as grinding time increased when high-grade quartz material is ground by vibratory disc and ball milling. While the highest $C_{av.}$ and the lowest $BRAR_{av.}$ values were determined by the longest grinding time for both mill type and size fractions, the more rounded particles were obtained by vibratory disc milling compared to ball milling for both size fractions as supported by *DIA* images.

Variation of average shape values with grinding time were correlated based on linear and exponential with power fitting models. It was concluded that, while linear model describes the $C_{av.}$ data for both mill and size fractions better than alternative fitting model (exponential fitting for $C_{av.}$ and power fitting for $1/BRAR_{av.}$), the $BRAR_{av.}$ data for both mill and size fractions were well represented by the alternative fitting model (exponential fitting for $C_{av.}$ and power fitting for $1/BRAR_{av.}$) considering the highest R^2 value, the lowest error% values and the reasonable required grinding

time for hypothetically spherical particles. When the prediction of average shape ($C_{av.}$ and $BRAR_{av.}$) values from the established mathematical models were made and compared with the experimental values, predicted values and experimental values of $C_{av.}$ and $BRAR_{av.}$ were closely related to each other along with acceptable R^2 values. Although laboratory mills such as vibratory disc and ball mill were used in this study, other grinding parameters (mill size, fill amount etc.) in other milling systems needs to be investigated. This approach provides useful insights into the prediction of the required grinding times for a suitable milling system for intended use. Since grinding is energy and cost intensive process, this approach is expected to be applicable to industrial scale mills and other particulate samples in a similar manner.

Acknowledgement

The authors thank to Professor Zhiyong Gao, who is a professional editor at Physicochemical Problems of Mineral Processing, for checking of the revised manuscript regarding English language and grammar.

Disclosure statement

No potential conflict of interest was reported by the author(s).

Nomenclature

<i>A</i>	the area of the particle image
<i>BRAR</i>	bounding rectangular aspect ratio
$BRAR_{av.}$	average value of bounding rectangular aspect ratio
<i>C</i>	circularity
$C_{av.}$	average value of circularity
D_{BC}	bounding circle diameter
<i>DIA</i>	dynamic image analysis
<i>sd</i>	shape distribution

ORCID

Ugur Ulusoy  <http://orcid.org/0000-0002-2634-7964>
Guler Bayar  <http://orcid.org/0000-0002-9060-4443>

References

- Allen, T. 1997. *Particle size measurement, volume 1, Powder sampling and particle size measurement*. 5th ed. Netherlands: Springer.
- Austin, L. G., and P. Bagga. 1981. An analysis of fine dry grinding in ball mills. *Powder Technology* 28 (1):83–90. doi:10.1016/0032-5910(81)87014-3.
- Choi, H., J. Lee, H. Hong, J. Gu, J. Lee, H. Yoon, J. Choi, Y. Jeong, J. Song, M. Kim, et al. 2013. New evaluation method for the kinetic analysis of the grinding rate constant via the uniformity of particle size distribution during a grinding process. *Powder Technology* 247: 44–6. doi:10.1016/j.powtec.2013.06.031.
- Ciullo, P. A. 1996. *Industrial minerals and their uses: A handbook and formulary*. 1st ed. Norwich, NY: William Andrew Publishing/Noyes.
- Dehghani, F., M. Rahimi, and B. Rezai. 2012. Influence of particle shape on the flotation of magnetite, alone and in the presence of quartz particles. *Journal of the Southern African Institute of Mining and Metallurgy* 113 (12):905–11.
- Güven, O., F. Karakas, N. Kodrazi, and M. S. Çelik. 2016. Dependence of morphology on anionic flotation of alumina. *International Journal of Mineral Processing* 156:69–74. doi:10.1016/j.minpro.2016.06.006.

- Hiçyılmaz, C., U. Ulusoy, and M. Yekeler. 2004. Effects of the shape properties of talc and quartz particles on the wettability based separation processes. *Applied Surface Science* 233 (1–4):204–12. doi:10.1016/j.apsusc.2004.03.209.
- Kaya, E., R. Hogg, and S. R. Kumar. 2002. Particle shape modification in comminution. *KONA Powder and Particle Journal* 20 (0):188–95. doi:10.14356/kona.2002021.
- Koh, P. T. L., F. P. Hao, L. K. Smith, T. T. Chau, and W. J. Bruckard. 2009. The effect of particle shape and hydrophobicity in flotation. *International Journal of Mineral Processing* 93 (2):128–34. doi:10.1016/j.minpro.2009.07.007.
- Little, L., A. N. Mainza, M. Becker, and J. Wiese. 2017. Fine grinding: How mill type affects particle shape characteristics and mineral liberation. *Minerals Engineering* 111:148–57. doi:10.1016/j.mineng.2017.05.007.
- Ma, G., W. Xia, and G. Xie. 2018. Effect of particle shape on the flotation kinetics of fine coking coal. *Journal of Cleaner Production* 195: 470–5. doi:10.1016/j.jclepro.2018.05.230.
- Micromeritics 2013. Particle Insight 1.00 Manual. Norcross, GA: Micromeritics® Instrument Corp.
- Mitchell, C. J. 2015. UK Frac sand resources. In *Proceedings of the 18th Extractive Industry Geology Conference*. *Extractive Industry Geology*, eds. E. Hunger, T. Brown and G. Lucas, 21–30. University of St. Andrews, Scotland: Wardrop Minerals Management Ltd. Publication.
- Mowla, D., G. Karimi, and K. Ostadnezhad. 2008. Removal of hematite from silica sand ore by reverse flotation technique. *Separation and Purification Technology* 58 (3):419–23. doi:10.1016/j.seppur.2007.08.023.
- Nguyen, A. V., and H. J. Schulze. 2004. *Colloidal science of flotation*. New York: Marcel Dekker.
- Ofori-Sarpong, G., and R. K. Amankwah. 2011. Comminution environment and gold particle morphology: Effects on gravity concentration. *Minerals Engineering* 24 (6):590–2. doi:10.1016/j.mineng.2011.02.014.
- Petrakis, E., V. Karmali, G. Bartzas, and K. Komnitsas. 2019. Grinding kinetics of slag and effect of final particle size on the compressive strength of alkali activated materials. *Minerals* 9 (11):714. doi:10.3390/min9110714.
- Rahimi, M., F. Dehghani, B. Rezai, and M. R. Aslani. 2012. Influence of the roughness and shape of quartz particles on their flotation kinetics. *International Journal of Minerals, Metallurgy, and Materials* 19 (4):284–9. doi:10.1007/s12613-012-0552-z.
- Sayilgan, A., and A. I. Arol. 2004. Effect of carbonate alkalinity on flotation behavior of quartz. *International Journal of Mineral Processing* 74 (1–4):233–8. doi:10.1016/j.minpro.2003.12.002.
- Sekulic, Z., N. Canic, Z. Bartulovic, and A. Dakovic. 2004. Application of different collectors in flotation concentration of feldspar, mica and quartz sand. *Minerals Engineering* 17:77–80.
- Teke, E., M. Yekeler, U. Ulusoy, and M. Canbazoglu. 2002. Kinetics of dry grinding of industrial minerals: Calcite and Barite. *International Journal of Mineral Processing* 67 (1–4):29–42. doi:10.1016/S0301-7516(02)00006-6
- Trahar, W. J., and L. J. Warren. 1976. The probability of very fine particles: A review. *International Journal of Mineral Processing* 3 (2): 103–31. doi:10.1016/0301-7516(76)90029-6.
- Tuncuk, A., and A. Akcil. 2014. Removal of iron from quartz ore using different acids: A laboratory-scale reactor study. *Mineral Processing and Extractive Metallurgy Review* 35 (4):217–28. doi:10.1080/08827508.2013.825614.
- Ulusoy, U. 2019. Quantifying of particle shape differences of differently milled barite using a novel technique: Dynamic image analysis. *Materialia* 8: 100434.
- Ulusoy, U. 2018. Dynamic image analysis of differently milled talc particles and comparison by various methods. *Particulate Science and Technology* 36 (3):332–9. doi:10.1080/02726351.2016.1248261.
- Ulusoy, U., and C. Igathinathane. 2014. Dynamic image based shape analysis of hard and lignite coal particles ground by laboratory ball and gyro mills. *Fuel Processing Technology* 126:350–8. doi:10.1016/j.fuproc.2014.05.017.
- Ulusoy, U., and C. Igathinathane. 2016. Particle size distribution modeling of milled coals by dynamic image analysis and mechanical sieving. *Fuel Processing Technology* 143:100–9. doi:10.1016/j.fuproc.2015.11.007.
- Ulusoy, U., and M. Yekeler. 2014. Dynamic image analysis of calcite particles created by different mills. *International Journal of Mineral Processing* 133:83–90. doi:10.1016/j.minpro.2014.10.006.
- Ulusoy, U., M. Yekeler, and C. Hicyılmaz. 2003. Determination of the shape, morphological and wettability properties of quartz and their correlations. *Minerals Engineering* 16 (10):951–64. doi:10.1016/j.mineng.2003.07.002.
- Unland, G. 2007. The principles of single-particle crushing. Chapter 4, vol 12. In *Handbook of powder technology*, eds. A. Salman, M. Ghadiri, and M. Hounslow, 117–225. Amsterdam: Elsevier.
- Verrelli, D. I., W. J. Bruckard, P. T. L. Koh, M. P. Schwarz, and B. Follink. 2014. Particle shape effects in flotation. Part 1: Microscale experimental observations. *Minerals Engineering* 58 (4):80–9. doi:10.1016/j.mineng.2014.01.004.
- Vision Analytical Inc. 2020. Application note: AN-004, how particle shape analysis impacts manufacturing process and final product.
- Vision Analytical Inc. 2021. Particle measurement technologies. <https://particleshape.com/particle-measurement-technologies> (accessed October 13, 2021).
- Wang, S., H. Fan, H. He, L. Tang, and X. Tao. 2020. Effect of particle shape and roughness on the hydrophobicity of low-rank coal surface. *International Journal of Coal Preparation and Utilization* 40 (12):876–91. doi:10.1080/19392699.2017.1423066.
- Wang, Y. H., and J. W. Ren. 2005. The flotation of quartz from iron minerals with a combined quaternary ammonium salt. *International Journal of Mineral Processing* 77:116–22.
- Wotruba, H., H. Hoberg, and F. U. Schneider. 1991, September 23–28. Investigation on the separation of microlithe and zircon. The influence of particle shape on floatability. Vol. 4. In *XVII. International Mineral Processing Congress*, H. Schubert and E. Forssberg, eds., 83. Dresden, Germany: Bergakademie Freiberg.
- Yekeler, M., A. Özkan, and L. G. Austin. 2001. Kinetics of fine wet grinding in a laboratory ball mill. *Powder Technology* 114 (1–3): 224–8. doi:10.1016/S0032-5910(00)00326-0.